Journal of Electronics and Electrical Engineering
https://ojs.wiserpub.com/index.php/JEEE

Research Article

Modeling and Analysis of Multiconductor Transmission Lines by Distributed Transfer Function Method

Bingen Yang

Department of Aerospace and Mechanical Engineering, University of Southern California, Los Angeles, CA, USA
E-mail: bingen@usc.edu

Received: 13 September 2024; **Revised:** 15 November 2024; **Accepted:** 22 November 2024

Abstract: Multiconductor transmission lines (MCTLs) have various applications in electrical engineering. In modeling and analysis of MCTLs, which are described by a set of coupled partial differential equations, most existing methods rely on approximation or discretization. For high-speed high-frequency applications, accurate analytical methods are always desirable. Such a method, however, is not currently available for complex MCTLs. This paper presents an innovative analytical method for modeling and analysis of MCTLs with various configurations. The proposed method, which is called the Distributed Transfer Function Method, is capable of delivering closed-form analytical solutions for complex MCTLs, in both the frequency domain and the time domain. One highlight of the proposed method is that it gives exact and closed-form solutions for branched transmission lines for the first time. The accuracy, efficiency, and high-frequency utility of the method is demonstrated in numerical examples.

***Keywords*:** multiconductor transmission lines, multiline systems, branched transmission lines, distributed transfer function method, analytical solutions, high-frequency analysis

1. Introduction

Multiconductor transmission lines (MCTLs) have various applications in electrical engineering, including electric power transmission, electronic devices, communication, high-speed circuits, antennas, and very large-scale integration (VLSI) technology [1, 2, 3, 4]. The current investigation is concerned with modeling and analysis of complex MCTLs that are assembled with three configurations: (i) cascaded transmission lines; (ii) coupled transmission lines; and (iii) branched transmission lines. A cascaded configuration is commonly seen in multi-section transmission lines for impedance matching in design of microwave systems. A coupled configuration arises from the phenomenon of crosstalk. A branched configuration is often considered in multiport transmission lines for multichannel communication. Mathematically, a multiconductor transmission line is described by a set of coupled partial differential equations.

For simplicity of presentation, an MCTL is also called a multiline system. A demonstrative multiline system is shown in Figure 1, where seven nodes (1, 2, …, 7) define the boundaries of the five transmission lines, and i_k denotes the current in the kth line. At Node 2, Lines 1 and 2 are in cascade connection. Node 2 is also a port with an impedance Z_p and a voltage input $v_p(t)$. Such a port describes a transmitter or receiver in a communication application. The dashed area represents the coupling between Lines 4 and 5 due to crosstalk, showing a coupled configuration. At Node 3, Lines 2, 3

DOI: https://doi.org/10.37256/jeee.3220245717

and 4 are interconnected, exhibiting a branched configuration. Also, at Nodes 1, 4, 5, 6 and 7, the boundary conditions with sources and load impedances can be specified. The multiline system in Figure 1 is a combination of the aforementioned three configurations.

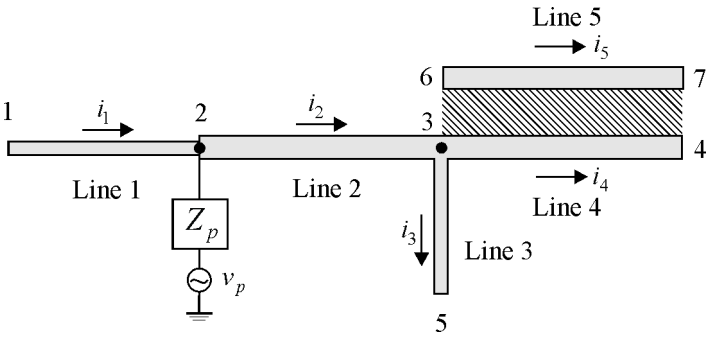

Figure 1. Schematic of a multiline system

In modeling and analysis of MCTLs, numerical methods are mostly applied, including the finite difference methods [5, 6, 7, 8], finite element methods [9, 10], numerical inverse Laplace transform [11, 12, 13], modal analysis [14], and hybrid finite element-wavelet expansion methods [15, 16]. For design of multichannel interconnects with high-frequency carriers, a closed-form model in the frequency domain was developed based on some approximation [17]. Besides numerical methods, semi-analytical methods for time-domain analysis were proposed. In Reference [18], by finite difference approximation in the spatial coordinate, the governing partial differential equations of a coupled nonuniform multiline system are reduced to a set of ordinary differential equations, which are then solved analytically. In Reference [19], through introduction of truncated Tayler series in inverse Laplace transform, a closed-form transient response of coupled transmission lines is obtained. The above-mentioned numerical and semi-analytical methods have found utilities in development and design of MCTLs.

In recent years, MCTL models have been widely adopted in a variety of engineering applications. Examples include circuits for antennas [20, 21], onboard electric wiring on aircraft [22], design of couplers, filters, and transmitters [23], transformers design [24], the track circuit in a railway signal system [25], and cable lines in power transmission systems [26, 27, 28]. In these applications, the aforementioned numerical and approximate methods were applied to obtain the dynamic response of the multiline systems in consideration.

Instead of the rich literature, modeling and analysis of MCTLs mostly relays on numerical and approximate methods. To the best of the author's knowledge, exact and analytical solution methods are currently unavailable for complex MCTLs, especially for branched multiline systems. An analytical method for complex MCTLs that can deliver highly accurate results and provide deep physical insights is certainly desirable, particularly in high-speed high-frequency applications. The development of such a modeling and analysis method should significantly benefit the design of many electronic devices and electrical systems, which, nevertheless, has not been well addressed in the past. The current investigation is motivated by the need to fill this technical gap in research and development.

This paper presents a new analytical method, namely the Distributed Transfer Function Method (DTFM), for modeling, synthesis, and analysis of multiconductor transmission lines. The DTFM was originally developed for vibration problems of elastic continua [29, 30, 31, 32]. In this work, the DTFM is extended to the problems of MCTLs. The proposed method, as the first of its own kind, does not require any approximation or discretization, and it can systematically deliver analytical solutions for complex MCTLs, in both the frequency and time domains. One highlight of the DTFM is that it obtains exact and closed-form solutions for branched transmission lines, which are currently unavailable in the literature. As shall be seen, the DTFM-based analysis is potentially useful for high-speed high-frequency applications.

The remainder of the paper is organized as follows. In Section 2, the DTFM is developed for single transmission lines to prepare for modeling and analysis of complex MCTLs. To this end, a distributed transfer function formulation and a

residue formula for inverse Laplace transform are derived, which eventually lead to frequency and time responses in closed form. By generalizing the DTFM-based analysis in Section 2, the responses of cascaded transmission lines and coupled transmission lines are determined in Sections 3 and 4, respectively. In Section 5, through introduction of an augmented state-space formulation, exact and closed-form responses of general MCTLs with branched configuration are obtained. In Section 6, for validation and comparison purposes, a numerical integration algorithm is derived. The proposed DTFM is demonstrated in two numerical examples in Section 7. Finally, the main results obtained in this study are summarized in Section 8.

2. Response of a single transmission line by DTFM

To prepare for modeling, synthesis, and analysis of multiline systems with the three configurations as mentioned in Section 1, in this section, the dynamic problem of a single transmission line (TL) is formulated and solved by the Distributed Transfer Function Method (DTFM). With the DTFM, the dynamic responses of the TL are obtained in exact and closed form. While the DTFM-based modeling and analysis is new even for a single TL, it lays out a foundation for the development of the proposed analytical method for complex MCTLs, as shall be seen in Sections 3 to 5.

2.1 *Spatial state-space formulation*

Consider a single TL shown in Figure 2, where $v(x,t)$ and $i(x,t)$ are the distributed voltage and current over the line; and l is the line length. Without loss of generality, assume zero initial voltage and current. According to the transmission line theory [1, 2], the TL are governed by the s-domain differential equations:

$$\begin{aligned} \frac{\partial \bar{v}(x,s)}{\partial x} &= -(Ls+R)\bar{i}(x,s) \\ \frac{\partial \bar{i}(x,s)}{\partial x} &= -(Cs+G)\bar{v}(x,s) \end{aligned} \tag{1}$$

for $0 < x < l$. Here, the overbar stands for Laplace transformation, such as $\bar{v}(x,s) = \mathscr{L}[v(x,t)]$ and $\bar{i}(x,s) = \mathscr{L}[i(x,t)]$, with $\mathscr{L}$ being the Laplace transform operator and s the complex Laplace transform parameter; and R, L, G and C are the unit length resistance, inductance, conductance and capacitance of the TL, respectively. The boundary conditions of the line are

$$\begin{aligned} &\text{at } x = 0: \quad Z_S(s)\bar{i}(0,s) = \bar{v}_s(s) - \bar{v}(0,s) \\ &\text{at } x = l: \quad Z_L(s)\bar{i}(l,s) = \bar{v}(l,s) \end{aligned} \tag{2}$$

where $\bar{v}_s(s)$ is the Laplace transform of the applied voltage $v_s(t)$ at the left end; and $Z_S(s)$ and $Z_L(s)$ are the source and load impedances.

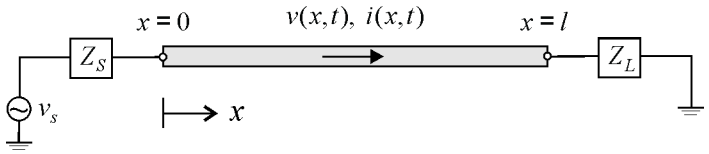

Figure 2. A single transmission line

To determine the response of the TL by the DTFM, define a state vector as follows

$$\hat{\boldsymbol{\eta}}(x,s) = \begin{pmatrix} \bar{v}(x,s) \\ \bar{i}(x,s) \end{pmatrix}, \quad x \in [0,\, l] \tag{3}$$

With the so defined state vector, Equations (1) and (2) are converted to the following spatial state-space formulation [29, 30]

$$\begin{array}{ll} \text{State equation:} & \frac{\partial}{\partial x}\hat{\boldsymbol{\eta}}(x,s) = \mathbf{F}(s)\hat{\boldsymbol{\eta}}(x,s), \quad 0 < x < l \\ \text{Boundary condition:} & \mathbf{M}_b(s)\hat{\boldsymbol{\eta}}(0,s) + \mathbf{N}_b(s)\hat{\boldsymbol{\eta}}(l,s) = \hat{\boldsymbol{\gamma}}_b(s) \end{array} \tag{4}$$

where

$$\begin{gathered} \mathbf{F}(s) = \begin{bmatrix} 0 & -(Ls+R) \\ -(Cs+G) & 0 \end{bmatrix}, \quad \hat{\boldsymbol{\gamma}}_b(s) = \begin{pmatrix} \bar{v}_s(s) \\ 0 \end{pmatrix} \\ \mathbf{M}_b(s) = \begin{bmatrix} 1 & Z_S(s) \\ 0 & 0 \end{bmatrix}, \quad \mathbf{N}_b(s) = \begin{bmatrix} 0 & 0 \\ -1 & Z_L(s) \end{bmatrix} \end{gathered} \tag{5}$$

2.2 *Exponential matrix*

The exponential matrix of the state-space formulation given by Equation (4) plays an important role in the DTFM-based analysis. By the method of matrix deposition [33], the exponential matrix $e^{\mathbf{F}(s)x}$ is obtained in the following analytical form

$$e^{\mathbf{F}(s)x} = \begin{bmatrix} \cosh(\sigma(s)x) & -\beta(s)\sinh(\sigma(s)x) \\ -\frac{1}{\beta(s)}\sinh(\sigma(s)x) & \cosh(\sigma(s)x) \end{bmatrix} \tag{6}$$

where

$$\sigma(s) = \sqrt{(Ls+R)(Cs+G)},\ \beta(s) = \sqrt{\frac{Ls+R}{Cs+G}} \tag{7}$$

which are known as the propagation constant and characteristic impedance of the TL, respectively.

2.3 *Eigenvalue problem*

The eigenvalue problem of the TL is described by the homogeneous state equation

$$\frac{\partial}{\partial x}\hat{\boldsymbol{\eta}}(x,s) = \mathbf{F}(s)\hat{\boldsymbol{\eta}}(x,s), \quad 0 < x < l \tag{8}$$

subject to the homogeneous boundary condition

$$\mathbf{M}_b(s)\hat{\boldsymbol{\eta}}(0,s) + \mathbf{N}_b(s)\hat{\boldsymbol{\eta}}(l,s) = 0 \tag{9}$$

where s is an eigenvalue and $\hat{\boldsymbol{\eta}}(x,s)$ is the associated eigenvector in the state-space form. Equation (8) can be simply obtained from Equation (4) by dropping $\hat{\boldsymbol{\gamma}}_b(s)$.

A nontrivial solution of Equation (8) is of the form [34],

$$\hat{\boldsymbol{\eta}}(x,s) = e^{\mathbf{F}(s)x}\boldsymbol{\eta}_0 \tag{10}$$

where $\boldsymbol{\eta}_0$ is a nonzero constant vector. Substituting Equation (10) into the boundary condition (9) gives the following homogenous equation

$$\left[\mathbf{M}_b(s)+\mathbf{N}_b(s)e^{\mathbf{F}(s)l}\right]\boldsymbol{\eta}_0=0 \tag{11}$$

To have a nontrivial solution $\boldsymbol{\eta}_0$, we must have

$$\Delta(s)\equiv\det\left[\mathbf{M}_b(s)+\mathbf{N}_b(s)e^{\mathbf{F}(s)l}\right]=0 \tag{12}$$

Equation (12) is a transcendental characteristic equation of s, which has an infinite number of roots as the eigenvalues of the TL.

Denote the eigenvalues of the TL by $s_{\pm k}$, $k=1,2,....$ For a lossless TL, its eigenvalues are imaginary, $s_{\pm k}=\pm j\omega_k$, where $j=\sqrt{-1}$, and ω_k are nonnegative real numbers. For a lossy TL, its eigenvalues are of the complex form $s_{\pm k}=-\sigma_k\pm j\omega_k$, where σ_k and ω_k are nonnegative real numbers. The roots can be determined by standard root-finding algorithms.

2.4 *Transfer function formulation and steady-state response*

The solution of Equation (4) takes the form [29, 30]

$$\hat{\boldsymbol{\eta}}(x,s)=\hat{\mathbf{H}}(x,s)\hat{\boldsymbol{\gamma}}_b(s),\quad 0<x<l \tag{13}$$

where $\hat{\mathbf{H}}(x,s)$ is the distributed transfer function of the TL and it is given by

$$\hat{\mathbf{H}}(x,s)=e^{\mathbf{F}(s)x}\mathbf{Z}_b^{-1}(s) \tag{14}$$

with

$$\mathbf{Z}_b(s)=\mathbf{M}_b(s)+\mathbf{N}_b(s)e^{\mathbf{F}(s)l} \tag{15}$$

With Equation (15), the characteristic Equation (12) can be written as $\det\mathbf{Z}_b(s)=0$, indicating that the poles of the transfer function $\hat{\mathbf{H}}(x,s)$ are the eigenvalues of the TL. Equation (13) is known as the distributed transfer function formulation for the line.

Consider a harmonic boundary voltage excitation $v_s(t)=E_0e^{j\omega t}$, where $j=\sqrt{-1}$, and E_0 and ω are the amplitude and frequency of the excitation. By Equation (14), the sinusoidal steady-state response of the TL is obtained as

$$\boldsymbol{\eta}_{ss}(x,t)=\begin{pmatrix} v_{ss}(x,t)\\ i_{ss}(x,t)\end{pmatrix}=\begin{pmatrix} V(x,\omega)\\ I(x,\omega)\end{pmatrix}e^{j\omega t} \tag{16}$$

where $v_{ss}(x,t)$ and $i_{ss}(x,t)$ are the steady-state voltage and current; and $V(x,\omega)$ and $I(x,\omega)$ are the frequency response functions of the line given by

$$\begin{pmatrix} V(x,\omega)\\ I(x,\omega)\end{pmatrix}=E_0\hat{\mathbf{H}}(x,j\omega)\begin{pmatrix}1\\0\end{pmatrix} \tag{17}$$

2.5 *Time response*

By performing inverse Laplace transform of Equation (13) with respect to time, the time response of the TL is given by

$$\boldsymbol{\eta}(x,t) = \begin{pmatrix} v(x,t) \\ i(x,t) \end{pmatrix} = \int_0^t \mathbf{H}(x,t-\tau) v_s(\tau) d\tau \begin{pmatrix} 1 \\ 0 \end{pmatrix}, \quad 0 < x < l \tag{18}$$

where $\boldsymbol{\eta}(x,t)$ is the inverse Laplace transform of the state vector $\hat{\boldsymbol{\eta}}(x,s)$; $\mathbf{H}(x,t)$ is the Green's function of the TL and it is the inverse Laplace transform of the transfer function $\hat{\mathbf{H}}(x,s)$.

By following Reference [31], the Green's function can be written as follows

$$\mathbf{H}(x,t) = \sum_{k=\pm 1}^{\pm\infty} e^{\mathbf{F}(s_k)x} \mathbf{Re}_k e^{s_k t} \tag{19}$$

where s_k is the kth eigenvalue of the TL; and $\mathbf{Re}_k$ is the transfer function residue at s_k and it is defined by

$$\mathbf{Re}_k = \operatorname*{Res}_{s=s_k} \left[\mathbf{Z}_b^{-1}(s) \right] \tag{20}$$

with $\mathbf{Z}_b(s)$ given in Equation (15). Subsuming Equation (19) into Equation (18) yields the time response of the TL in the following infinite series:

$$\boldsymbol{\eta}(x,t) = \sum_{k=\pm 1}^{\pm\infty} e^{\mathbf{F}(s_k)x} \mathbf{Re}_k \int_0^t e^{s_k(t-\tau)} v_s(\tau) d\tau \begin{pmatrix} 1 \\ 0 \end{pmatrix} \tag{21}$$

Given a load $v_s(t)$, the integral in Equation (21) can be evaluated by exact quadrature.

The key in the transient analysis by the infinite series (21) is to determine the transfer function residues. The transfer function residue at s_k can be written as [35, 36]

$$\mathbf{Re}_k = \frac{\text{adj}\mathbf{Z}_b(s_k)}{\frac{d}{ds}|\mathbf{Z}_b(s)|_{s=s_k}} \tag{22}$$

where $|\mathbf{Z}_b| = \det \mathbf{Z}_b$, and $\text{adj}\mathbf{Z}_b$ is the adjoint of $\mathbf{Z}_b$. Note that $\mathbf{F}(s), \mathbf{M}_b(s)$ and $\mathbf{N}_b(s)$ are two-by-two matrices. By matrix theory, it is easy to show that

$$\begin{aligned} \frac{d}{ds}|\mathbf{Z}_b(s)| = &\left| \frac{d\mathbf{M}_b(s)}{ds} + \mathbf{N}_b(s) e^{\mathbf{F}(s)l} \right| + \left| \mathbf{M}_b(s) + \frac{d\mathbf{N}_b(s)}{ds} e^{\mathbf{F}(s)l} \right| \\ &+ \left| \mathbf{M}_b(s) + \mathbf{N}_b(s) \frac{de^{\mathbf{F}(s)l}}{ds} \right| \end{aligned} \tag{23}$$

With Equations (6) and (7), it can be shown that

$$\frac{de^{\mathbf{F}(s)l}}{ds} \equiv \boldsymbol{\Phi}(s) = \begin{bmatrix} \phi_{11}(s) & \phi_{12}(s) \\ \phi_{21}(s) & \phi_{22}(s) \end{bmatrix} \tag{24}$$

where

$$\begin{aligned}\phi_{11}(s) &= \phi_{22}(s) = l\sinh(\sigma(s)l)\,\tfrac{d\sigma(s)}{ds}\\ \phi_{12}(s) &= -\sinh(\sigma(s)l)\,\tfrac{d\beta(s)}{ds} - \beta(s)l\cosh(\sigma(s)l)\,\tfrac{d\sigma(s)}{ds}\\ \phi_{21}(s) &= \tfrac{1}{\beta^2(s)}\sinh(\sigma(s)l)\,\tfrac{d\beta(s)}{ds} - \tfrac{l}{\beta(s)}\cosh(\sigma(s)x)\,\tfrac{d\sigma(s)}{ds}\end{aligned} \tag{25}$$

with

$$\frac{d\sigma(s)}{ds} = \frac{2LCs+LG+RC}{2\sigma(s)}, \quad \frac{d\beta(s)}{ds} = \frac{1}{2\sigma(s)}\frac{LG-CR}{(Cs+G)} \tag{26}$$

In summary of this section, by the distributed transfer function formulation (13) and the residue formula described by Equations (22)–(26), the frequency and time responses of the TL are obtained in exact and closed form. The results presented here are readily extensible to MCTLs in the subsequent sections.

3. Analysis of multi-section transmission lines

Multi-section transmission lines (MSTLs), which are also called multi-segment or cascaded transmission lines, exhibit one of the three configurations as mentioned in Section 1. In this section, the DTFM-based modeling and analysis presented in Section 2 is extended to MSTLs. The keys in the developments are the spatial state-space equations and the distributed transfer function formulation.

3.1 *Spatial state-space equations*

An MSTL consisting of n serially connected sections of transmission lines is shown in Figure 3, where the numbers in paratheses, (1), (2), …, (n), indicate the section numbers; $x_1, x_2, \ldots, x_{n-1}$ are the interior nodes, where two adjacent sections are interconnected; and x_0 and x_n are the boundary nodes where the source and load are specified. All the nodes are described in a global coordinate x, such that $x_0 < x_1 < x_2 < \cdots < x_n$.

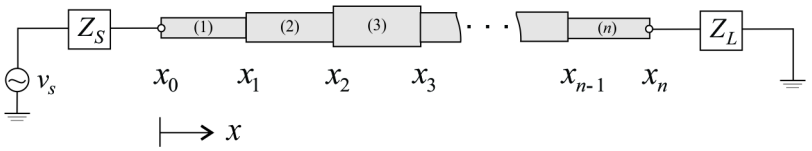

Figure 3. An n-section transmission line

Without loss of generality, assume zero initial conditions on the voltage and current of each section. In the Laplace transform domain, the governing equations of the kth section are

$$\begin{aligned}\frac{\partial \bar{v}_k(x,s)}{\partial x} &= -(L_k s + R_k)\bar{i}_k(x,s)\\ \frac{\partial \bar{i}_k(x,s)}{\partial x} &= -(C_k s + G_k)\bar{v}_k(x,s)\end{aligned} \tag{27}$$

for $x \in (x_{k-1}, x_k)$, where $\bar{v}_k(x,s)$ and $\bar{i}_k(x,s)$ are the voltage and current of the section. According to Figure 3, the boundary conditions of the MSTL are specified as follows

$$\begin{aligned}&\text{at } x = x_0: \quad Z_S(s)\bar{i}_1(x_0,s) = \bar{v}_s(s) - \bar{v}(x_0,s)\\ &\text{at } x = x_n: \quad Z_L(s)\bar{i}(x_n,s) = \bar{v}(x_n,s)\end{aligned} \tag{28}$$

The matching conditions at the interior nodes, by KVL and KCL, are given as

$$\begin{aligned} \bar{i}_{j+1}(x_j,s) &= \bar{i}_j(x_j,s) \\ \bar{v}_{j+1}(x_j,s) &= \bar{v}_j(x_j,s) \end{aligned} \tag{29}$$

for $j = 1,2,...,n-1$.

Define the state vectors of the sections as follows

$$\hat{\boldsymbol{\eta}}_k(x,s) = \begin{pmatrix} \bar{v}_k(x,s) \\ \bar{i}_k(x,s) \end{pmatrix}, \quad x \in [x_{k-1},x_k], \quad k = 1,2,...,n \tag{30}$$

By following Section 2, Equations (27)–(29) are converted to the following state-space form

(a) State equations:

$$\frac{\partial}{\partial x}\hat{\boldsymbol{\eta}}_k(x,s) = \mathbf{F}_k(x,s)\hat{\boldsymbol{\eta}}_k(x,s), \quad x \in [x_{k-1},x_k], \quad k = 1,2,...,n \tag{31}$$

(b) Boundary condition

$$\mathbf{M}_b(s)\hat{\boldsymbol{\eta}}_1(x_0,s) + \mathbf{N}_b(s)\hat{\boldsymbol{\eta}}_n(x_n,s) = \hat{\boldsymbol{\gamma}}_b(s) \tag{32}$$

(c) Matching conditions

$$\hat{\boldsymbol{\eta}}_{j+1}(x_j,s) = \hat{\boldsymbol{\eta}}_j(x_j,s), \quad j = 1,2,...,n-1 \tag{33}$$

Here,

$$\begin{aligned} \mathbf{F}_k(s) &= \begin{bmatrix} 0 & -(L_k s + R_k) \\ -(C_k s + G_k) & 0 \end{bmatrix}, \quad k = 1,2,...,n \\ \mathbf{M}_b(s) = \begin{bmatrix} 1 & Z_S(s) \\ 0 & 0 \end{bmatrix}, \quad \mathbf{N}_b(s) &= \begin{bmatrix} 0 & 0 \\ -1 & Z_L(s) \end{bmatrix}, \quad \hat{\boldsymbol{\gamma}}_b(s) = \begin{pmatrix} \bar{v}_s(s) \\ 0 \end{pmatrix} \end{aligned} \tag{34}$$

3.2 *System response*

The solutions of the state equations given by Equation (31) are of the form

$$\hat{\boldsymbol{\eta}}_k(x,s) = e^{\mathbf{F}_k(s)(x-x_{k-1})}\mathbf{a}_k, \quad x \in [x_{k-1},x_k], \quad k = 1,2,...,n \tag{35}$$

where $\mathbf{a}_k$ are constant vectors to be determined. The exponential matrices of the sections can be obtained by following Equation (6). With Equation (35) and by the matching conditions (33),

$$\mathbf{a}_{j+1} = e^{\mathbf{F}_j(s)l_j}\mathbf{a}_j, \quad j = 1,2,...,n-1 \tag{36}$$

where $l_j = x_j - x_{j-1}$, which is the length of the jth section. It follows that

$$\mathbf{a}_{j+1} = e^{\mathbf{F}_j(s)l_j}e^{\mathbf{F}_{j-1}(s)l_{j-1}}\cdots e^{\mathbf{F}_1(s)l_1}\mathbf{a}_1, \quad j = 1,2,...,n-1 \tag{37}$$

Substituting Equations (35) and (37) into the boundary condition (32) gives

$$\mathbf{Z}_b(s)\mathbf{a}_1 = \hat{\boldsymbol{\gamma}}_b(s) \tag{38}$$

where

$$\mathbf{Z}_b(s) = \mathbf{M}_b(s) + \mathbf{N}_b(s)\boldsymbol{\Psi}(s) \tag{39}$$

with

$$\boldsymbol{\Psi}(s) = e^{\mathbf{F}_n(s)l_n} e^{\mathbf{F}_{n-1}(s)l_{n-1}} \cdots e^{\mathbf{F}_2(s)l_2} e^{\mathbf{F}_1(s)l_1} \tag{40}$$

With the state-space formulation described by Equations (35)–(40), the solutions of the eigenvalues, frequency response and time response of the MSTL are obtained as follows.

(A) Eigenvalues

The characteristic equation of the MSTL, by Equation (38) with $\hat{\boldsymbol{\gamma}}_b(s) = 0$, is

$$\Delta(s) \equiv \det \mathbf{Z}_b(s) = \det\left[\mathbf{M}_b(s) + \mathbf{N}_b(s)\boldsymbol{\Psi}(s)\right] = 0 \tag{41}$$

from which the eigenvalues (roots s_k) can be determined.

(B) Frequency Response

Define a global state vector

$$\hat{\boldsymbol{\eta}}(x,s) = \hat{\boldsymbol{\eta}}_k(x,s), \quad x \in [x_{k-1}, x_k], \quad k = 1,2,...,n \tag{42}$$

Let the total length of the MSTL be $l_T = l_1 + l_2 + \cdots + l_n = x_n - x_0$. From Equation (38),

$$\mathbf{a}_1 = \mathbf{Z}_b^{-1}(s)\hat{\boldsymbol{\gamma}}_b(s) \tag{43}$$

It follows from Equations (35) and (43) that the s-domain response of the MSTL is

$$\hat{\boldsymbol{\eta}}(x,s) = \hat{\mathbf{H}}(x,s)\hat{\boldsymbol{\gamma}}_b(s), \quad 0 < x < l_T \tag{44}$$

Where the distributed transfer function is given by

$$\hat{\mathbf{H}}(x,s) = e^{\mathbf{F}_k(s)(x-x_{k-1})} e^{\mathbf{F}_{k-1}(s)l_{k-1}} \cdots e^{\mathbf{F}_1(s)l_1} \mathbf{Z}_b^{-1}(s), \quad \text{for } x \in [x_{k-1}, x_k] \tag{45}$$

Note that the transfer function formulation (44) is the same in format as given in Equation (13). Thus, under a harmonic boundary excitation $v_s(t) = E_0 e^{j\omega t}$, the sinusoidal steady-state response of the MSTL can be presented by Equations (16) and (17), except that $\hat{\mathbf{H}}(x, j\omega)$ is computed by using Equation (45). Thus, the frequency response of the multi-section line is obtained in closed form without approximation.

(C) Time Response

By following Section 2.5, inverse Laplace transform of Equation (44) and use of the residue formula [31] gives the closed-form time response of the MSTL as follows

$$\boldsymbol{\eta}(x,t)=\sum_{k=\pm1}^{\pm\infty} e^{\mathbf{F}_j(s_k)(x-x_{j-1})}e^{\mathbf{F}_{j-1}(s_k)l_{j-1}}\cdots e^{\mathbf{F}_1(s_k)l_1}\mathbf{Re}_k\int_0^t e^{s_k(t-\tau)}v_s(\tau)d\tau\begin{pmatrix}1\\0\end{pmatrix} \tag{46}$$

for $x\in[x_{k-1},x_k]$, $k=1,2,...,n$, where s_k are the eigenvalues of the line, which are the roots of the characteristic Equation (41); and $\mathbf{Re}_k$ are the transfer function residues specified in Equation (22). It is easy to show that the derivative $d\left|\mathbf{Z}_b(s)\right|/ds$ in Equation (22) for the MSTL is given by

$$\begin{aligned}\tfrac{d}{ds}\left|\mathbf{Z}_b(s)\right| = &\left|\tfrac{d\mathbf{M}_b(s)}{ds}+\mathbf{N}_b(s)\boldsymbol{\Psi}(s)\right|+\left|\mathbf{M}_b(s)+\tfrac{d\mathbf{N}_b(s)}{ds}\boldsymbol{\Psi}(s)\right|\\&+\left|\mathbf{M}_b(s)+\mathbf{N}_b(s)\tfrac{d\boldsymbol{\Psi}(s)}{ds}\right|\end{aligned} \tag{47}$$

where, by the chain rule,

$$\begin{aligned}\tfrac{d\boldsymbol{\Psi}(s)}{ds} = &\tfrac{de^{\mathbf{F}n(s)l_n}}{ds}e^{\mathbf{F}_{n-1}(s)l_{n-1}}\cdots e^{\mathbf{F}_1(s)l_1}+e^{\mathbf{F}_n(s)l_n}\tfrac{de^{\mathbf{F}_{n-1}(s)l_{n-1}}}{ds}\cdots e^{\mathbf{F}_1(s)l_1}\\&+\cdots+e^{\mathbf{F}_n(s)l_n}e^{\mathbf{F}_{n-1}(s)l_{n-1}}\cdots\tfrac{de^{\mathbf{F}_1(s)l_1}}{ds}\end{aligned} \tag{48}$$

The analytical expressions of $de^{\mathbf{F}_j(s)l_j}/ds$ can be obtained by following Equations (24)–(26). Thus, the closed-form time response of the MSTL can be obtained by Equations (46) to (48).

4. Analysis of coupled transmission lines

In this section, the DTFM-based modeling and analysis as presented in Section 2 is extended to coupled transmission lines, which is another configuration as mentioned in Section 1.

In a crosstalk phenomenon, undesired capacitive, indicative and conductive coupling between two or more transmission lines occurs. Consider two coupled transmission lines of equal length that are parallel and close to each other. The coupling of the lines is described by the following s-domain matrix differential Equation [3, 37]

$$\begin{aligned}\tfrac{\partial\hat{\mathbf{V}}(x,s)}{\partial x}+(\mathbf{Ls}+\mathbf{R})\hat{\mathbf{I}}(x,s)=0\\ \tfrac{\partial\hat{\mathbf{I}}(x,s)}{\partial x}+(\mathbf{Cs}+\mathbf{G})\hat{\mathbf{V}}(x,s)=0\end{aligned} \tag{49}$$

for $0<x<l$, where

$$\hat{\mathbf{V}}(x,s)=\begin{pmatrix}\bar{v}_1(x,s)\\ \bar{v}_2(x,s)\end{pmatrix},\quad \hat{\mathbf{I}}(x,s)=\begin{pmatrix}\bar{i}_1(x,s)\\ \bar{i}_2(x,s)\end{pmatrix} \tag{50}$$

with $\bar{v}_k(x,s)$ and $\bar{i}_k(x,s)$ being the voltage and current of the kth line; and $\mathbf{L}$, $\mathbf{R}$, $\mathbf{C}$ and $\mathbf{G}$ are two-by-two matrices of per-unit-length inductance, resistance, capacitance and conductance, respectively. For instance, the inductance and capacitance matrices may be of the form

$$\mathbf{L}=\begin{bmatrix}L_1 & L_m\\ L_m & L_2\end{bmatrix},\quad \mathbf{C}=\begin{bmatrix}C_1+C_m & -C_m\\ -C_m & C_2+C_m\end{bmatrix} \tag{51}$$

where L_m and C_m are the mutual inductance and capacitance per unit length, characterizing the coupling of the lines.

The boundary of the coupled system are

$$\begin{aligned} &\text{at } x=0: \quad \mathbf{A}_0(s)\hat{\mathbf{V}}(0,s)+\mathbf{B}_0(s)\hat{\mathbf{I}}(0,s)=\hat{\mathbf{p}}_0(s) \\ &\text{at } x=l: \quad \mathbf{A}_l(s)\hat{\mathbf{V}}(0,s)+\mathbf{B}_l(s)\hat{\mathbf{I}}(l,s)=\hat{\mathbf{p}}_l(s) \end{aligned} \tag{52}$$

where $\mathbf{A}_0(s), \mathbf{B}_0(s), \mathbf{A}_l(s)$ and $\mathbf{B}_l(s)$ are two-by-two matrices describing boundary impedances; and $\hat{\mathbf{p}}_0(s)$ and $\hat{\mathbf{p}}_l(s)$ are vectors of boundary excitations.

Define the state vector of the coupled system by

$$\hat{\boldsymbol{\eta}}(x,s)=\begin{pmatrix} \hat{\mathbf{V}}(x,s) \\ \hat{\mathbf{I}}(x,s) \end{pmatrix} \in C^4, \quad x\in[0,\ l] \tag{53}$$

Equations (49) and (52) are cast into the spatial state-space formulation (4), with

$$\begin{aligned} \mathbf{F}(s)&=\begin{bmatrix} 0 & -(\mathbf{L}s+\mathbf{R}) \\ -(\mathbf{C}s+\mathbf{G}) & 0 \end{bmatrix} \\ \mathbf{M}_b(s)=\begin{bmatrix} \mathbf{A}_0(s) & \mathbf{B}_0(s) \\ 0 & 0 \end{bmatrix}, \quad \mathbf{N}_b(s)&=\begin{bmatrix} 0 & 0 \\ \mathbf{A}_l(s) & \mathbf{B}_l(s) \end{bmatrix}, \quad \hat{\gamma}_b(s)=\begin{pmatrix} \hat{\mathbf{p}}_0(s) \\ \hat{\mathbf{p}}_l(s) \end{pmatrix} \end{aligned} \tag{54}$$

Accordingly, the closed-form solutions of the coupled system can be obtained by following Section 2. The eigenvalues of the coupled system can be determined by solving Equation (12) and the frequency response can be obtained by following Equation (16), with the quantities given in Equation (54). A time response of the coupled system can be obtained by using Equation (21). The transfer function residues are still given by following Equation (22). However, the expression of $\frac{d}{ds}|\mathbf{Z}_b(s)|_{s=s_k}$ given by Equation (23) is invalid because $\mathbf{Z}_b(s)$ is a matrix of order four for the coupled system. According to Jacobi's formula in matrix calculus [38],

$$\frac{d}{ds}|\mathbf{Z}_b(s)|=\mathrm{tr}\left(\mathrm{adj}\mathbf{Z}_b(s)\frac{d\mathbf{Z}_b(s)}{ds}\right) \tag{55}$$

where $\mathrm{adj}\mathbf{Z}_b$ is the adjoint of $\mathbf{Z}_b$ and $\mathrm{tr}(\mathbf{A})$ is the trace of a square matrix $\mathbf{A}$; and

$$\frac{d\mathbf{Z}_b(s)}{ds}=\frac{d\mathbf{M}_b(s)}{ds}+\frac{d\mathbf{N}_b(s)}{ds}e^{\mathbf{F}(s)L}+\mathbf{N}_b(s)\frac{d}{ds}\left[e^{\mathbf{F}(s)l}\right] \tag{56}$$

An analytical form of $d\left[e^{\mathbf{F}(s)l}\right]/ds$ can be obtained by following Section 2.5. Thus, the closed-form time response of the coupled line system can be obtained.

Although only two coupled lines are considered, with some modifications, the formulas presented in this section can be extended the coupled system with more than two lines.

5. Synthesis and analysis of branched multiline systems

In many applications multiple transmission lines are assembled with a branched configuration, rendering a multibody problem that is described in a set of interconnected subregions (see Figure 1 for instance). For such a multibody problem, conventional analytical methods cannot deliver closed-form solutions without approximation. In this section, the proposed DTFM, with an augmented state-space formulation, is shown to be able to deliver exact and closed-form solutions for branched multiline systems for the first time.

5.1 *System description*

For demonstrative purposes, we consider the multiline system in Figure 1, which is a combination of cascaded, coupled and branched configurations. For convenience of description, a local coordinate for each line is used. The local spatial coordinate x of the kth line is in the direction of i_k, varying from 0 to l_k (the length of the line). In other words, the origin of the local coordinate is at Node 1 for Line 1, Node 2 for Line 2, Node 3 for Lines 3 and 4, and Node 6 for Line 5.

In many problems, the dynamic response of a multiline system is caused by loads (say, voltage inputs) at its nodes, which are boundary excitations. Hence, without loss of generality, zero initial currents and voltages of the transmission lines are assumed in this work. (The free response of the multiline system due to initial disturbances can be determined by following the reference [31]). With this assumption, the s-domain governing equations of the lines are given by [1, 2]

$$\begin{aligned} \frac{\partial \bar{v}_k(x,s)}{\partial x} &= -(L_k s + R_k)\bar{i}_k(x,s) + \bar{v}_{e,k}(x,s) \\ \frac{\partial \bar{i}_k(x,s)}{\partial x} &= -(C_k s + G_k)\bar{v}_k(x,s) + \bar{i}_{e,k}(x,s) \end{aligned} \tag{57}$$

for $x \in (0, l_k)$ and k = 1, 2 and 3 (Lines 1, 2 and 3), and

$$\begin{aligned} \frac{\partial \bar{\mathbf{v}}_c(x,s)}{\partial x} &= -(\mathbf{L}_c s + \mathbf{R}_c)\bar{\mathbf{i}}_c(x,s) \\ \frac{\partial \bar{\mathbf{i}}_c(x,s)}{\partial x} &= -(\mathbf{C}_c s + \mathbf{G}_c)\bar{\mathbf{v}}_c(x,s) \end{aligned} \tag{58}$$

for $x \in (0, l_4)$ and k = 4 and 5 (Lines 4 and 5), with

$$\bar{\mathbf{v}}_c(x,s) = \begin{pmatrix} \bar{v}_4(x,s) \\ \bar{v}_5(x,s) \end{pmatrix}, \quad \bar{\mathbf{i}}_c(x,s) = \begin{pmatrix} \bar{i}_4(x,s) \\ \bar{i}_5(x,s) \end{pmatrix} \tag{59}$$

where $\mathbf{L}_c$, $\mathbf{R}_c$, $\mathbf{C}_c$ and $\mathbf{G}_c$ are two-by-two parameter matrices that are similar to those in Equation (49). In the previous equations, the overbar stands for Laplace transformation; and Lines 4 and 5 have the equal length, $l_4 = l_5$.

The boundary conditions of the multiline system are specified as follows

$$\begin{aligned} &\text{at Node 1 :} && a_1\bar{v}_1(0,s) + b_1\bar{i}_1(0,s) = \bar{q}_1(s) \\ &\text{at Node 4 :} && a_4\bar{v}_4(l_4,s) + b_4\bar{i}_4(l_4,s) = \bar{q}_4(s) \\ &\text{at Node 5 :} && a_5\bar{v}_3(l_3,s) + b_5\bar{i}_3(l_3,s) = \bar{q}_5(s) \\ &\text{at Node 6 :} && a_6\bar{v}_5(0,s) + b_6\bar{i}_5(0,s) = \bar{q}_5(s) \\ &\text{at Node 7 :} && a_7\bar{v}_5(l_5,s) + b_7\bar{i}_5(l_5,s) = \bar{q}_7(s) \end{aligned} \tag{60}$$

where $\bar{q}_k(s)$ are the boundary excitations, and coefficients a_k and b_k in general can be functions of s. The matching conditions at Node 2, by KVL and KCL, are written as follows

$$\begin{aligned} \bar{v}_1(l_1,s) &= \bar{v}_2(0,s) \\ \bar{i}_1(l_1,s) - \bar{i}_2(0,s) &= \tfrac{1}{Z_p(s)}\{\bar{v}_1(l_1,s) - \bar{v}_p(s)\} \end{aligned} \tag{61}$$

where $\bar{v}_p(s)$ is the Laplace transform of $v_p(t)$, and $Z_p(s)$ is the impedance at the node (port). The matching conditions at Node 3, at which three lines are interconnected, are given by

$$\begin{aligned} \bar{v}_2(l_2,s) &= \bar{v}_3(0,s) = \bar{v}_4(0,s) \\ \bar{i}_2(l_2,s) &= \bar{i}_3(0,s) + \bar{i}_4(0,s) \end{aligned} \tag{62}$$

5.2 *Augmented state-space formulation*

Equations (57) and (58) are described in five interconnected subregions of different lengths, $(0, l_k)$, $k = 1, 2, ..., 5$. For such a multibody (multi-region) problem, it is difficult to obtain exact analytical solutions by conventional methods. In this work, an augmented state-space formulation is introduced such that the multibody problem is reduced to the format of a single-body problem as described in Section 2, which then can be solved by the DTFM. This approach is called the augmented Distributed Transfer Function Method [32].

Define a nondimensional coordinate z for each line by

$$z = \frac{x}{l_k}, \quad k = 1, 2, ..., 5 \tag{63}$$

which has the same direction as x and varies in the range $0 \leq z \leq 1$. With the coordinate transformation (63), Equation (57) is converted to

$$\begin{array}{l} \frac{\partial \bar{v}_k(z,s)}{\partial z} = -l_k(L_k s + R_k)\bar{i}_k(z,s) \\ \frac{\partial \bar{i}_k(z,s)}{\partial z} = -l_k(C_k s + G_k)\bar{v}_k(z,s) \end{array} \tag{64}$$

for k = 1, 2 and 3, and Equation (58) is converted to

$$\begin{array}{l} \frac{\partial \bar{\mathbf{v}}_c(z,s)}{\partial z} = -l_3\left(\mathbf{L}_c s + \mathbf{R}_c\right)\bar{\mathbf{i}}_c(z,s) \\ \frac{\partial \bar{\mathbf{i}}_c(z,s)}{\partial z} = -l_3\left(\mathbf{C}_c s + \mathbf{G}_c\right)\bar{\mathbf{v}}_c(z,s) \end{array} \tag{65}$$

In the previous equations, the coordinate z is universal for all the lines; and $\bar{v}_k(z,s) = \bar{v}_k(x,s)|_{x=l_k z}$ and $\bar{i}_k(z,s) = \bar{i}_k(x,s)|_{x=l_k z}$. Similarly, the boundary conditions (60) are reduced to

$$\begin{array}{ll} \text{at Node 1 :} & a_1\bar{v}_1(0,s) + b_1\bar{i}_1(0,s) = \bar{q}_1(s) \\ \text{at Node 4 :} & a_4\bar{v}_4(1,s) + b_4\bar{i}_4(1,s) = \bar{q}_4(s) \\ \text{at Node 5 :} & a_5\bar{v}_3(1,s) + b_5\bar{i}_3(1,s) = \bar{q}_5(s) \\ \text{at Node 6 :} & a_6\bar{v}_5(0,s) + b_6\bar{i}_5(0,s) = \bar{q}_5(s) \\ \text{at Node 7 :} & a_7\bar{v}_5(1,s) + b_7\bar{i}_5(1,s) = \bar{q}_7(s) \end{array} \tag{66}$$

and the matching conditions (61) and (62) are reduced to

$$\begin{array}{ll} \text{at Node 2} & \bar{v}_1(1,s) = \bar{v}_2(0,s) \\ & Z_p(s)\left(\bar{i}_1(1,s) - \bar{i}_2(0,s)\right) = \bar{v}_1(1,s) - \bar{v}_p(s) \\ \text{at Node 3} & \bar{v}_2(1,s) = \bar{v}_3(0,s) = \bar{v}_4(0,s) \\ & \bar{i}_2(1,s) = \bar{i}_3(0,s) + \bar{i}_4(0,s) \end{array} \tag{67}$$

Define the state vectors for Lines 1 to 3 by

$$\hat{\boldsymbol{\eta}}_k(z,s) = \begin{pmatrix} \bar{v}_k(z,s) \\ \bar{i}_k(z,s) \end{pmatrix} \in C^2, \quad z \in [0,1], \quad k = 1,2,3 \tag{68}$$

Define the state vector for the coupled lines (Lines 4 and 5) by

$$\hat{\boldsymbol{\eta}}_c(z,s) = \begin{pmatrix} \bar{v}_c(z,s) \\ \bar{i}_c(x,s) \end{pmatrix} \in C^4, \quad z \in [0,1] \tag{69}$$

The state equations for Lines 1 to 3 are obtained from (64) as follows

$$\frac{\partial}{\partial z}\hat{\boldsymbol{\eta}}_k(z,s) = \mathbf{F}_k(s)\hat{\boldsymbol{\eta}}_k(z,s), \quad z \in (0,1), \quad k = 1,2,3 \tag{70}$$

with

$$\mathbf{F}_k(s) = -l_k \begin{bmatrix} 0 & L_k s + R_k \\ C_k s + G_k & 0 \end{bmatrix} \tag{71}$$

For the coupled lines, the state equation is obtained from Equation (66) as follows

$$\frac{\partial}{\partial z}\hat{\boldsymbol{\eta}}_c(z,s) = \mathbf{F}_c(s)\hat{\boldsymbol{\eta}}_c(z,s), \quad z \in (0,1) \tag{72}$$

where

$$\mathbf{F}_c(s) = -l_4 \begin{bmatrix} \mathbf{0} & \mathbf{L}_c s + \mathbf{R}_c \\ \mathbf{C}_c s + \mathbf{G}_c & \mathbf{0} \end{bmatrix} \tag{73}$$

Now, introduce a global state vector for the branched multiline system by

$$\hat{\boldsymbol{\eta}}(z,s) = \begin{pmatrix} \hat{\boldsymbol{\eta}}_1(z,s) \\ \hat{\boldsymbol{\eta}}_2(z,s) \\ \hat{\boldsymbol{\eta}}_3(z,s) \\ \hat{\boldsymbol{\eta}}_c(z,s) \end{pmatrix} \in C^{10}, \quad z \in [0,1] \tag{74}$$

Assembly of Equations (70) and (72) yields a global state equation as follows

$$\frac{\partial}{\partial z}\hat{\boldsymbol{\eta}}(z,s) = \mathbf{F}_G(s)\hat{\boldsymbol{\eta}}(z,s), \quad z \in (0,1) \tag{75}$$

where

$$\mathbf{F}_G(s) = \text{diag}\left\{ \begin{array}{cccc} \mathbf{F}_1(s), & \mathbf{F}_2(s), & \mathbf{F}_3(s), & \mathbf{F}_c(s) \end{array} \right\} \in C^{10\times 10} \tag{76}$$

Also, the boundary conditions (66) and matching conditions (67) are converted to the following global boundary condition

$$\mathbf{M}_G(s)\hat{\boldsymbol{\eta}}(0,s) + \mathbf{N}_G(s)\hat{\boldsymbol{\eta}}(1,s) = \hat{\boldsymbol{\gamma}}_G(s) \tag{77}$$

where

$$\mathbf{M}_G(s) = \begin{bmatrix} \mathbf{M}_b(s) \\ \mathbf{M}_m(s) \end{bmatrix}, \quad \mathbf{N}_G(s) = \begin{bmatrix} \mathbf{N}_b(s) \\ \mathbf{N}_m(s) \end{bmatrix}, \quad \hat{\boldsymbol{\gamma}}_G(s) = \begin{pmatrix} \hat{\boldsymbol{\gamma}}_b(s) \\ \hat{\boldsymbol{\gamma}}_m(s) \end{pmatrix} \tag{78}$$

with

$$
\mathbf{M}_b(s)=\begin{bmatrix} a_1 & b_1 & 0 & 0 & 0 & 0 & 0 & 0 & 0 & 0 \\ 0 & 0 & 0 & 0 & 0 & 0 & 0 & 0 & 0 & 0 \\ 0 & 0 & 0 & 0 & 0 & 0 & 0 & 0 & 0 & 0 \\ 0 & 0 & 0 & 0 & 0 & 0 & 0 & a_6 & 0 & b_6 \\ 0 & 0 & 0 & 0 & 0 & 0 & 0 & 0 & 0 & 0 \end{bmatrix}
$$

$$
\mathbf{N}_b(s)=\begin{bmatrix} 0 & 0 & 0 & 0 & 0 & 0 & 0 & 0 & 0 & 0 \\ 0 & 0 & 0 & 0 & 0 & 0 & a_4 & 0 & b_4 & 0 \\ 0 & 0 & 0 & 0 & a_5 & b_5 & 0 & 0 & 0 & 0 \\ 0 & 0 & 0 & 0 & 0 & 0 & 0 & 0 & 0 & 0 \\ 0 & 0 & 0 & 0 & 0 & 0 & 0 & a_7 & 0 & b_7 \end{bmatrix}, \quad \hat{\gamma}_b(s)=\begin{pmatrix} \bar{q}_1(s) \\ \bar{q}_4(s) \\ \bar{q}_5(s) \\ \bar{q}_6(s) \\ \bar{q}_7(s) \end{pmatrix}
$$

$$
\mathbf{M}_m(s)=\begin{bmatrix} 0 & 0 & -1 & 0 & 0 & 0 & 0 & 0 & 0 & 0 \\ 0 & 0 & 0 & Z_p(s) & 0 & 0 & 0 & 0 & 0 & 0 \\ 0 & 0 & 0 & 0 & -1 & 0 & 0 & 0 & 0 & 0 \\ 0 & 0 & 0 & 0 & 0 & 0 & -1 & 0 & 0 & 0 \\ 0 & 0 & 0 & 0 & 0 & -1 & 0 & 0 & -1 & 0 \end{bmatrix}
$$

$$
\mathbf{N}_m(s)=\begin{bmatrix} 1 & 0 & 0 & 0 & 0 & 0 & 0 & 0 & 0 & 0 \\ 1 & -Z_p(s) & 0 & 0 & 0 & 0 & 0 & 0 & 0 & 0 \\ 0 & 0 & 1 & 0 & 0 & 0 & 0 & 0 & 0 & 0 \\ 0 & 0 & 1 & 0 & 0 & 0 & 0 & 0 & 0 & 0 \\ 0 & 0 & 0 & 1 & 0 & 0 & 0 & 0 & 0 & 0 \end{bmatrix}, \quad \hat{\gamma}_m(s)=\begin{pmatrix} 0 \\ \bar{v}_p(s) \\ 0 \\ 0 \\ 0 \end{pmatrix} \tag{79}
$$

Equations (75) and (77) are known as an *augmented state-space formulation*. With this formulation, which does not depend on any discretization or approximation, the original multibody problem of the multiline system in Figure 1 is converted to a single-body problem defined over the region $0 \le z \le 1$. Consequently, the formulas presented in Section 2 for a single transmission line can be extended to the branched multiline system here.

5.3 *Eigenvalues and dynamic response by augmented DTFM*

After introducing a universal nondimensional coordinate z, the resulting Equations (75) and (77) have the same format as the state-space formulation given by Equation (4). Thus, the eigenvalues and dynamic response of a branched multiline system can be obtained by following Section 2.

The eigenvalues of the system, by following Equation (12), can be determined by solving the characteristic equation

$$
\Delta(s) \equiv \det \mathbf{Z}_G(s) = 0 \tag{80}
$$

where

$$
\mathbf{Z}_G(s) = \mathbf{M}_G(s) + \mathbf{N}_G(s) e^{\mathbf{F}_G(s)} \tag{81}
$$

The s-domain response of the system, by following Equation (13), is given by

$$
\hat{\boldsymbol{\eta}}(z,s) = \hat{\mathbf{H}}_G(z,s)\hat{\gamma}_G(s), \quad z \in (0,1) \tag{82}
$$

where the global distributed transfer function is

$$
\hat{\mathbf{H}}_G(z,s) = e^{\mathbf{F}_G(s)z}\mathbf{Z}_G^{-1}(s) \tag{83}
$$

Consider harmonic excitations described by

$$\boldsymbol{\gamma}_G(t) = \boldsymbol{\gamma}_0 e^{j\omega t}, \quad j = \sqrt{-1} \tag{84}$$

where $\boldsymbol{\gamma}_0$ is a constant vector. The sinusoidal steady-state response of the multiline system, by following Equations (16) and (17), is obtained as

$$\boldsymbol{\eta}_{ss}(x,t) = \hat{\mathbf{H}}_G(z, j\omega)\boldsymbol{\gamma}_0 e^{j\omega t}, \quad z \in (0,1) \tag{85}$$

where $\hat{\mathbf{H}}_G(z, j\omega)$ is the frequency response function of the system.

The time response of the MCTL, by following Equations (18) and (21), is given by the infinite series

$$\boldsymbol{\eta}(z,t) = \sum_{k=\pm 1}^{\pm\infty} e^{\mathbf{F}_G(s_k)z}\mathbf{Re}_k \int_0^t e^{s_k(t-\tau)}\boldsymbol{\gamma}_G(\tau)d\tau, \quad z \in (0,1) \tag{86}$$

where $\eta(x,t)$ is the inverse Laplace transform of $\hat{\boldsymbol{\eta}}(x,s)$; s_k are the eigenvalues of the system that are the roots of the characteristic Equation (80); and

$$\boldsymbol{\gamma}_G(t) = \begin{pmatrix} q_1(t) & q_4(t) & q_5(t) & q_6(t) & q_7(t) & 0 & v_p(t) & 0 & 0 & 0 \end{pmatrix}^T \tag{87}$$

with the elements being the inverse Laplace transforms of the elements of $\hat{\boldsymbol{\gamma}}_G(s)$ that are given in Equations (78) and (79). The transfer function residues $\mathbf{Re}_k$ in Equation (86) are given by

$$\mathbf{Re}_k = \frac{\text{adj}\mathbf{Z}_G(s_k)}{\frac{d}{ds}|\mathbf{Z}_G(s)|_{s=s_k}} = \frac{\text{adj}\mathbf{Z}_G(s_k)}{\text{tr}\left(\text{adj}\mathbf{Z}_G(s_k)\frac{d\mathbf{Z}_G(s_k)}{ds}\right)} \tag{88}$$

where Jacobi's formula in matrix calculus [38] has been used. Like in Equation (23), the evaluation of the derivative $d\mathbf{Z}_G(s_k)/ds$ requires the computation of $de^{\mathbf{F}_G(s)}/ds$. Because $\mathbf{F}_G(s)$ is of the block-diagonal form (76),

$$\frac{de^{\mathbf{F}_G(s)}}{ds} = \text{diag}\left\{ \frac{de^{\mathbf{F}_1(s)}}{ds}, \quad \frac{de^{\mathbf{F}_2(s)}}{ds}, \quad \frac{de^{\mathbf{F}_3(s)}}{ds}, \quad \frac{de^{\mathbf{F}_c(s)}}{ds} \right\} \tag{89}$$

where $de^{\mathbf{F}_k(s)}/ds$ and $de^{\mathbf{F}_c(s)}/ds$ can be estimated by following Section 2.5. Thus, with the formulas given by Equations (86) to (89), a closed-form time response of the multiline system can be obtained.

Although only a five-line system is considered in this section, the augmented DTFM presented is certainly applicable to general MCTLs.

6. Frequency response via numerical integration

The new analytical method (DTFM) for branched multiline systems is developed in the previous section. In this section, for validation purposes, the augmented state equations and boundary conditions, as presented in Section 5.2, are solved by the Euler's method, a first-order numerical integration algorithm. With the numerical integration, the frequency response of a branched multiline system is computed. The DTFM and the numerical integration method are compared in Section 7.

Divide the nondimensional region $0 \leq z \leq 1$ into n subintervals by $n+1$ equally spaced points: $z_k = kh$, with $h = 1/n$ and $k = 0, 1, 2, ..., n$. Define a sequence of state vectors by

$$\hat{\boldsymbol{\eta}}_k(s) = \hat{\boldsymbol{\eta}}(z_k, s) = \hat{\boldsymbol{\eta}}(kh, s), \quad k = 0, 1, 2, ..., n \tag{90}$$

With the Euler's method [39], Equation (75) is approximated as

$$\frac{1}{h}\left(\hat{\boldsymbol{\eta}}_{k+1}(s) - \hat{\boldsymbol{\eta}}_k(s)\right) = \mathbf{F}_G(s)\hat{\boldsymbol{\eta}}_k(s) \tag{91}$$

which leads to

$$\hat{\boldsymbol{\eta}}_{k+1}(s) = \left(\mathbf{I} + h\mathbf{F}_G(s)\right)\hat{\boldsymbol{\eta}}_k(s) \tag{92}$$

with $\mathbf{I}$ being an identity matrix. Recursive use of Equation (92) yields

$$\hat{\boldsymbol{\eta}}_k(s) = \boldsymbol{\Phi}_k(s)\hat{\boldsymbol{\eta}}_0(s), \quad k = 0, 1, 2, ..., n \tag{93}$$

where

$$\boldsymbol{\Phi}_k(s) = \left(\mathbf{I} + h\mathbf{F}_G(s)\right)^k \tag{94}$$

with $\boldsymbol{\Phi}_0(s) = \mathbf{I}$. With Equation (90), the boundary condition (77) can be written as

$$\mathbf{M}_G(s)\hat{\boldsymbol{\eta}}_0(s) + \mathbf{N}_G(s)\hat{\boldsymbol{\eta}}_n(s) = \hat{\boldsymbol{\gamma}}_G(s) \tag{95}$$

Substituting Equation (93) into Equation (95) gives

$$\left(\mathbf{M}_G(s) + \mathbf{N}_G(s)\boldsymbol{\Phi}_n(s)\right)\hat{\boldsymbol{\eta}}_0(s) = \hat{\boldsymbol{\gamma}}_G(s) \tag{96}$$

Thus,

$$\hat{\boldsymbol{\eta}}_0(s) = \left(\mathbf{M}_G(s) + \mathbf{N}_G(s)\boldsymbol{\Phi}_n(s)\right)^{-1}\hat{\boldsymbol{\gamma}}_G(s) \tag{97}$$

It follows from Equations (93) and (97) that the s-domain response of the system is given by

$$\hat{\boldsymbol{\eta}}_k(s) = \boldsymbol{\Phi}_k(s)\left(\mathbf{M}_G(s) + \mathbf{N}_G(s)\boldsymbol{\Phi}_n(s)\right)^{-1}\hat{\boldsymbol{\gamma}}_G(s), \quad k = 0, 1, 2, ..., n \tag{98}$$

Let the system be subject harmonic excitations, $\boldsymbol{\gamma}_G(t) = \boldsymbol{\gamma}_0 e^{j\omega t}$, as described in Equation (84). By following Equation (85), the steady-state response of the system is expressed by

$$\boldsymbol{\eta}_{ss}(z_k, t) = \boldsymbol{\eta}_{k,ss}(t) = \hat{\mathbf{H}}_k(\omega)\boldsymbol{\gamma}_0 e^{j\omega t}, \quad k = 0, 1, 2, ..., n \tag{99}$$

where $\hat{\mathbf{H}}_k(\omega)$ is the frequency response of the system at point z_k and it is given by

$$\hat{\mathbf{H}}_k(\omega) = \mathbf{\Phi}_k(j\omega)(\mathbf{M}_G(j\omega) + \mathbf{N}_G(j\omega)\mathbf{\Phi}_n(j\omega))^{-1} \tag{100}$$

Comparison of Equations (83) and (100) indicates that $\hat{\mathbf{H}}_k(\omega)$ is the approximation of $\hat{\mathbf{H}}_G(z_k, j\omega)$. The formula given by Equation (99) is also applicable to multi-section transmission lines (Section 3) and coupled transmission lines (Section 4).

7. Numerical examples

The proposed DTFM is illustrated on two transmission lines: a single transmission line (Section 7.1), whose eigenvalues and time response are obtained, and a three-line branched system (Section 7.2), whose frequency response at both low and high frequencies is computed. For validation and comparison, the numerical integration given in Section 6 is also used.

7.1 *A single transmission line*

Consider the transmission line shown in Figure 2, where $v_s(t)$ is an applied voltage at the left end of the line; and the source and load impedances are described by resistances: $Z_s = R_s$ and $Z_l = R_l$. Assume zero external and initial excitations over the domain of the line. The line is governed by Equation (1) and the boundary conditions

$$\begin{aligned} &\text{at } x = 0: \quad R_s i(0,t) = v_s(t) - v(0,t) \\ &\text{at } x = l: \quad R_l i(l,t) = v(l,t) \end{aligned} \tag{101}$$

The following non-dimensional system parameters are selected in simulation:

$$L = 2, \quad R = 0.1, \quad C = 1, \quad G = 0.02, \quad l = 1, \quad R_s = 0.1, \quad R_l = 80$$

In this example, the eigenvalues and time response of the line are computed.

The characteristic equation of the line is Equation (12), with $e^{\mathbf{F}(s)x}$ given in Equation (6) and

$$\mathbf{M}_b(s) = \begin{bmatrix} 1 & R_s \\ 0 & 0 \end{bmatrix}, \quad \mathbf{N}_b(s) = \begin{bmatrix} 0 & 0 \\ -1 & R_l \end{bmatrix} \tag{102}$$

The nonzero R, G, R_s and R_l mean that this is a lossy transmission line. Consequently, the eigenvalues of the line are complex with negative real parts. In this work, the eigenvalues of the line are determined by a root locus method described in the Appendix. Table 1 lists the first 10 eigenvalues of the line, where $\mathrm{i} = \sqrt{-1}$. The third column in the table gives the errors in the root-finding, where $\Delta(s)$ is the characteristic function given in Equation (12).

Table 1. First 10 eigenvalues of the transmission line

k	s_k	$\lvert\Delta(s_k)\rvert$
1	−9.7614e-02 + 1.1101e+00i	2.4524e-12
2	−9.7588e-02 + 3.3320e+00i	5.9712e-13
3	−9.7586e-02 + 5.5535e+00i	9.2038e-13
4	−9.7585e-02 + 7.7750e+00i	3.2117e-13
5	−9.7585e-02 + 9.9964e+00i	4.2461e-13
6	−9.7585e-02 + 1.2218e+01i	5.7843e-13
7	−9.7585e-02 + 1.4439e+01i	6.8134e-13
8	−9.7585e-02 + 1.6661e+01i	5.7204e-13
9	−9.7585e-02 + 1.8882e+01i	6.2402e-13
10	−9.7585e-02 + 2.1104e+01i	9.5048e-13

Let the applied voltage be of the form $v_s(t) = E_0(1 - e^{-\sigma t})$, with $E_0 > 0$ and $\sigma > 0$. According to Equation (21), the time response of the line is given by

$$\begin{pmatrix} v(x,t) \\ i(x,t) \end{pmatrix} = \int_0^t \mathbf{H}(x,t-\tau) v_s(\tau) d\tau \begin{pmatrix} 1 \\ 0 \end{pmatrix} = 2E_0 \sum_{k=1}^{\infty} \mathrm{Re}\left\{ e^{\mathbf{F}(s_k)x} \mathbf{Re}_k q_k(t) \right\} \begin{pmatrix} 1 \\ 0 \end{pmatrix} \tag{103}$$

where $\mathbf{Re}_k$ are the transfer function residues at s_k, which are computed by Equation (22), and

$$q_k(t) = \int_0^t e^{s_k(t-\tau)} \left(1 - e^{-\sigma\tau}\right) d\tau = \frac{1}{s_k + \sigma} \left(e^{-\sigma t} - e^{s_k t}\right) - \frac{1}{s_k} \left(1 - e^{s_k t}\right) \tag{104}$$

Because the eigenvalues of the line all have negative real parts (see Table 1) and because $\lim_{t\to\infty} v_s(t) = E_0$, by the final value theorem in Laplace transform [35, 36], the steady-state response of the line as t goes to infinity is obtained as follows

$$\begin{aligned} \begin{pmatrix} V_{ss}(x) \\ I_{ss}(x) \end{pmatrix} &\equiv \lim_{t\to\infty} \begin{pmatrix} v(x,t) \\ i(x,t) \end{pmatrix} = \lim_{s\to 0} s\hat{\mathbf{H}}(x,s) \bar{v}_s(s) \begin{pmatrix} 1 \\ 0 \end{pmatrix} \\ &= E_0 e^{\mathbf{F}(0)x} \mathbf{Z}_b^{-1}(0) \begin{pmatrix} 1 \\ 0 \end{pmatrix} \end{aligned} \tag{105}$$

where the transfer function formulation (13) has been used; and $V_{ss}(x)$ and $I_{ss}(x)$ are the spatial distributions of the steady-state voltage and current along the length of the transmission line.

Let the excitation parameters be $E_0 = 10$ and $\sigma = 2$. The first 200 terms in the series (103) are taken to compute the time response. In Figure 4, the voltage and current of the transmission line at the midpoint ($x = l/2 = 0.5$) are plotted for $0 \le t \le 40$. In the figure, the dashed lines indicate the steady-state values (final values) of $v(0.5,t)$ and $i(0.5,t)$, which by Equation (105) are estimated as $V_{ss}(0.5) = 9.9540$ and $I_{ss}(0.5) = 0.2238$. The transient voltage and current of the line eventually settle at their steady-state values. It is also seen that the voltage and current at $x = 0.5$ are zero during $0 \le t \le 0.7$. This is due to the wave propagation on the line: the wave speed can be roughly estimated as $c_w \approx 1/\sqrt{LC} = 0.71$ and it takes the time $t = x/c_w = 0.7$ for the waves to travel from the left end of the line to the midpoint.

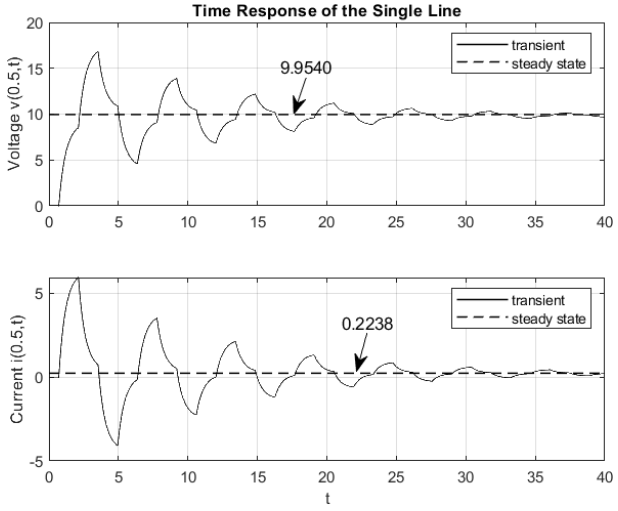

Figure 4. The voltage and current of the single line at the midpoint, for $0 \le t \le 40$s

7.2 *Frequency response of a branched multiline system*

A branched system of three transmission lines is shown in Figure 5, where at Node 1, a resistor R_s (source impedance) is attached and a voltage $v_s(t)$ is applied; at Node 2, the three lines are interconnected; and at Node 3, an LR series circuit is installed as the load. In this example, the frequency response of the branched system at both low and high frequencies are computed.

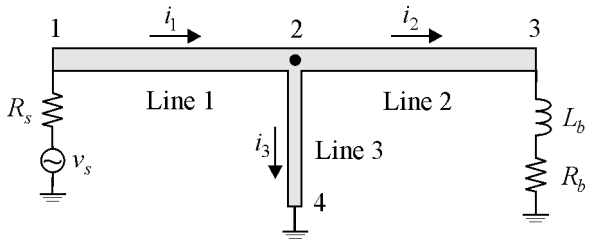

Figure 5. A branched system of three transmission lines

The branched multiline system is described by the global state Equation (75), with

$$\begin{gathered}\hat{\boldsymbol{\eta}}(z,s)=\begin{pmatrix}\hat{\boldsymbol{\eta}}_1(z,s)\\ \hat{\boldsymbol{\eta}}_2(z,s)\\ \hat{\boldsymbol{\eta}}_3(z,s)\end{pmatrix}, \quad z\in[0,1]\\ \mathbf{F}_G(s)=\underset{1\le k\le 3}{\operatorname{diag}}\{\mathbf{F}_k(s)\}, \quad \hat{\mathbf{q}}_G(z,s)=\mathbf{0}\end{gathered} \tag{106}$$

where z is a nondimensional local coordinate, and $\mathbf{F}_k(s)$ is given in Equation (71). The s-domain boundary conditions, in terms of z, are given by

$$\begin{aligned}&\text{at Node 1}: && R_s\bar{i}_1(0,s)=\bar{v}_s(s)-\bar{v}_1(0,s)\\ &\text{at Node 3}: && (L_bs+R_b)\bar{i}_2(1,s)=\bar{v}_2(1,s)\\ &\text{at Node 4}: && \bar{v}_3(1,s)=0\end{aligned} \tag{107}$$

The matching conditions at Node 2 are obtained as follows

$$\begin{aligned}\bar{v}_1(1,s)&=\bar{v}_2(0,s)=\bar{v}_3(0,s)\\ \bar{i}_1(1,s)&=\bar{i}_2(0,s)+\bar{i}_3(0,s)\end{aligned} \tag{108}$$

Assembly of the boundary and matching conditions gives the boundary condition (77), with

$$\begin{gathered}\mathbf{M}_G(s)=\begin{bmatrix}1&R_s&0&0&0&0\\0&0&0&0&0&0\\0&0&0&0&0&0\\0&0&-1&0&0&0\\0&0&0&0&-1&0\\0&0&0&-1&0&-1\end{bmatrix}, \quad \mathbf{N}_G(s)=\begin{bmatrix}0&0&0&0&0&0\\0&0&-1&L_bs+R_b&0&0\\0&0&0&0&1&0\\1&0&0&0&0&0\\1&0&0&0&0&0\\0&1&0&0&0&0\end{bmatrix}\\ \hat{\boldsymbol{\gamma}}_G(s)=\begin{pmatrix}\bar{v}_s(s)&0&0&0&0&0\end{pmatrix}^T\end{gathered} \tag{109}$$

Consider a harmonic excitation $v_s(t) = E_0 e^{j\omega t}$, $j = \sqrt{-1}$. The sinusoidal steady-state response of the branched system is obtained by Equation (85) as follows:

$$\boldsymbol{\eta}_{ss}(z,t) = E_0 \hat{\mathbf{H}}_G(z, j\omega)\mathbf{e}_1 e^{j\omega t}, \quad 0 \le z \le 1 \tag{110}$$

where $\mathbf{e}_1 = \begin{pmatrix} 1 & 0 & 0 & 0 & 0 & 0 \end{pmatrix}^T$, and

$$\hat{\mathbf{H}}(z,s) = e^{\mathbf{F}_G(s)z}\left(\mathbf{M}_G(s) + \mathbf{N}_G(s)e^{\mathbf{F}_G(s)}\right)^{-1} \tag{111}$$

From Equation (110), the sinusoidal steady-state response of each line can be determined. For instance, the steady-state voltage of Line 2 is

$$v_2(z,t) = E_0 V_2(z,\omega)e^{j\omega t}, \quad 0 \le z \le 1 \tag{112}$$

where $V_2(z,\omega)$ is a frequency response function of the line given by

$$V_2(z,\omega) \equiv \frac{v_2(z,t)}{E_0 e^{j\omega t}} = \mathbf{e}_3^T \hat{\mathbf{H}}_G(z, j\omega)\mathbf{e}_1 \tag{113}$$

with $\mathbf{e}_3 = \begin{pmatrix} 0 & 0 & 1 & 0 & 0 & 0 \end{pmatrix}^T$. By definition, the values of $V_2(z,\omega)$ are nondimensional.

For numerical simulation, assign the system parameters as follows

$$\begin{array}{lllllll} \text{Line 1:} & L_1 = 2\times10^{-7}\text{H}, & R_1 = 6\,\Omega, & C_1 = 2\times10^{-7}\text{F}, & G_1 = 0, & l_1 = 0.048\,\text{m} \\ \text{Line 2:} & L_2 = 1\times10^{-7}\text{H}, & R_2 = 10\,\Omega, & C_2 = 3\times10^{-7}\text{F}, & G_2 = 0, & l_2 = 0.04\,\text{m} \\ \text{Line 3:} & L_3 = 2\times10^{-7}\text{H}, & R_3 = 15\,\Omega, & C_3 = 4\times10^{-7}\text{F}, & G_3 = 0, & l_3 = 0.08\,\text{m} \\ \text{Boundaries:} & R_s = 100\,\Omega, & L_b = 0.1 & R_b = 500\,\Omega & & \end{array} \tag{114}$$

With Equation (113), the magnitudes of the steady-state voltage of the system at Nodes 2 and 3 are determined by the frequency response function of Line 2 as follows

$$\begin{aligned} M_2(\omega) &\equiv |V_2(0,\omega)| \\ M_3(\omega) &\equiv |V_2(1,\omega)| \end{aligned} \tag{115}$$

In Figure 6, $M_2(\omega)$ and $M_3(\omega)$ are plotted against ω for $0 \le \omega \le 90$ MHz. To validate the accuracy of the DTFM-based prediction, the Euler's method of numerical integration, as given by Equation (99), is applied to estimate the frequency response of the voltage at Node 3. The predication by the numerical integration is denoted by $\tilde{M}_3^n(\omega)$, where n is the number of subintervals. The $M_3(\omega)$ and $\tilde{M}_3^n(\omega)$ with n = 100, 200 and 400 are plotted in Figure 7, which indicates that the results by the Euler's method, as n increases, converge to that by the DTFM. It is also seen from the figure that the error of the numerical integration grows significantly at higher frequencies.

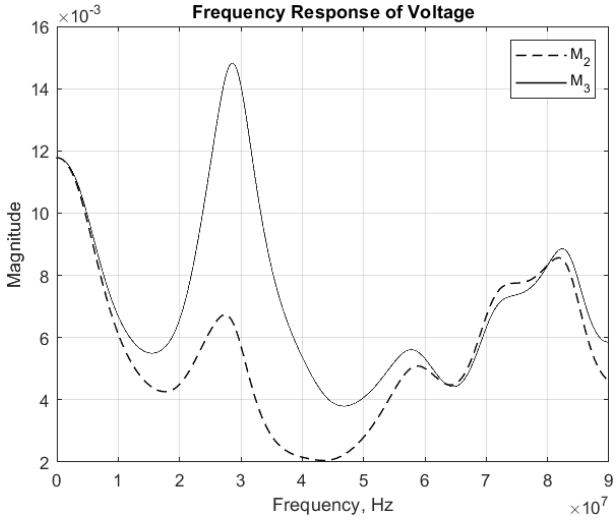

Figure 6. The magnitudes of the steady-state voltage at Nodes 2 and 3, from 0 to 90 MHz

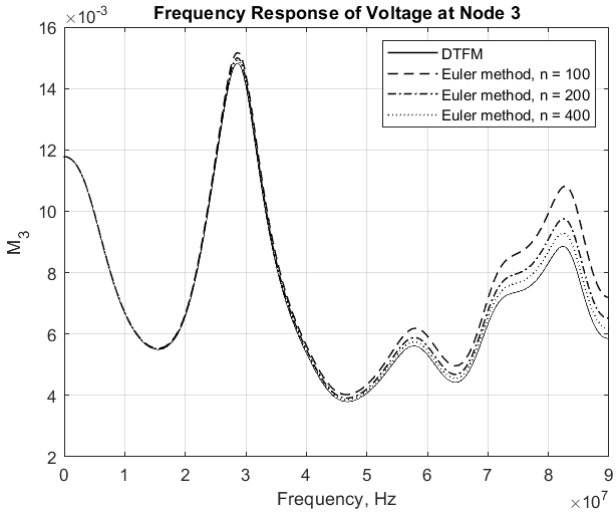

Figure 7. Comparison of the frequency response curves of the voltage at Node 3

As shown in Figure 7, the numerical integration with $n = 400$ may not be accurate enough at higher frequencies. To see this, define a relative error of the Euler's method by

$$\varepsilon_n = \max_{\omega_L \le \omega \le \omega_H} \left\{ \frac{\left| \tilde{M}_3^n(\omega) - M_3(\omega) \right|}{M_3(\omega)} \right\} \times 100\% \tag{116}$$

where n is the number of subintervals as mentioned previously, and ω_L and ω_H are the lower and upper bounds of a frequency region of interest. In the current example, $\omega_L = 0$ and $\omega_H = 90$ MHz. Table 2 lists the relative error for different values of n. As can be seen, 400 subintervals lead to an error of 5.6%, which may not be acceptable. To have an error of 1.5% or less, at least 1500 subintervals are required in the numerical integration.

Table 2. Relative error of the Euler's method for $0 \leq \omega \leq 90$ MHz (n = number of subintervals)

n	100	200	400	600	900	1500	2250
ε_n (%)	25.8	11.5	5.6	3.8	2.5	1.5	1.0

To show the utility of the DTFM in high-frequency applications, consider a frequency region from 5.0 GHz to 5.4 GHz. In Figure 8, the magnitudes of the steady-state voltage at Nodes 2 and 3 (M_2 and M_3) are plotted by Equation (113), which yields the exact solutions at the high frequencies. In this high-frequency simulation, the numerical integration by Equation (99) with a very large number of subintervals may not produce accurate results. This is shown in Table 3, where the relative error ε_n is defined by Equation (116), with ω_L = 5.0 GHz and ω_L = 5.4 GHz. As seen from the table, 200,000 subintervals lead to an error of 49.6%, and even with 1,000,000 subintervals, the use of Equation (99) still results in a relative error of 8.4%. It is also found from the simulation that for $n \leq 8000$, the matrices involved in the numerical integration become ill-conditioned and as such, a relative error could not be obtained. To have an error of 2% or less, at least 3,000,000 subintervals are required.

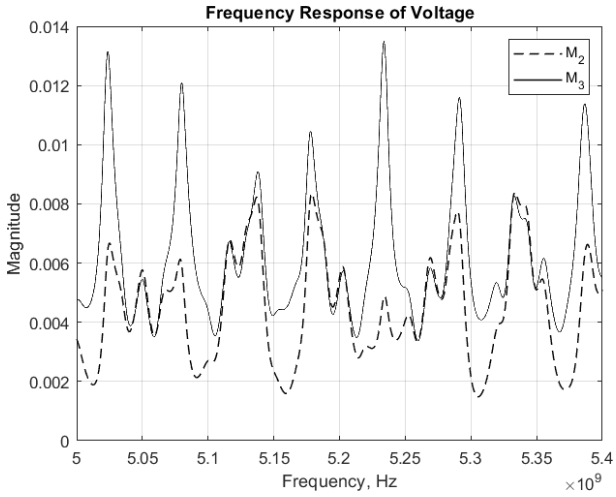

Figure 8. The magnitudes of the steady-state voltage at Nodes 2 and 3, from 5.0 to 5.4 GHz

Table 3. Relative error of the Euler's method for 5.0 GHz $\leq \omega \leq$ 5.4 GHz (n = number of subintervals)

n	$\leq$ 8000	200,000	1,000,000	2,000,000	3,000,000
ε_n (%)	N/A	49.6	8.4	4.1	2.0

As indicated by Table 3, to produce a high-frequency response of a multiline system by numerical methods, many unknowns need be determined, which requires significant computational effort. On the other hand, in the DTFM-based simulation, the same analytical formulas, such as Equation (110), can deliver exact solutions at both low and higher frequencies, with the same and least computational effort.

8. Conclusions

A new analytical method, namely the Distributed Transfer Function Method (DTFM), has been developed for modeling, synthesis and analysis of general multiconductor transmission lines (MCTLs). The main results from this investigation are summarized as follows.

(1) With an s-domain state-space formulation, the DTFM is applicable to MCTLs with cascaded, coupled, and branched configurations, and combinations. In the DTFM-based modeling and analysis, no approximation or discretization is required.

(2) The DTFM delivers analytical solutions for MCTLs in both the frequency domain and the time domain. As one highlight of this work, the proposed method gives exact closed-form solutions for branched transmission lines for the first time.

(3) The DTFM is highly efficient in computation. In particular, the proposed method can produce the high-frequency response of a branched MCTL, with ease and accuracy, as shown in the numerical example in Section 7.2. Because the same analytical formulas are usable at both low and high frequencies, the computational effort with the DTFM is essentially the same in any frequency region of interest. This unique feature renders the proposed method promising in high-speed and high-frequency applications.

Conflict of interest

There is no conflict of interest for this study.

Appendix: A Root Locus Method for Root-Finding

For the lossy transmission line in Section 7.1, consider a lossless line with $R = 0, G = 0$, and $R_S = R_L = 0$, which shall be called a reference line. This reference line is governed by the wave equation

$$LC\frac{\partial^2 v(x,t)}{\partial t^2} = \frac{\partial^2 v(x,t)}{\partial x^2}, \quad 0 < x < l \tag{A1}$$

subject to the boundary conditions $v(0,t) = v(l,t) = 0$. It is easy to show that the eigenvalues of the reference line are given by

$$s^{\circ}_{\pm k} = \pm j\frac{k\pi}{l\sqrt{LC}}, \quad j = \sqrt{-1}, \quad k = 1,2,.... \tag{A2}$$

In the characteristic Equation (12), replace the resistance and conductance parameters by variable parameters as follows:

$$R \to \mu R, \quad G \to \mu G, \quad R_S \to \mu R_S, \quad R_L \to \mu R_L \tag{A3}$$

where μ is a nondimensional parameter varying from 0 to 1. If $\mu = 0$, solution of Equation (12) yields the eigenvalues of the reference line as given by Equation (A2). If $\mu = 1$, solution of Equation (12) gives the eigenvalues of the original lossy line. Now vary μ in N steps:

$$\mu = \mu_n = n\Delta\mu, \quad \Delta\mu = 1/N, \quad n = 1,2,...,N \tag{A4}$$

where N is an integer that is large than one. (For the TL in Section 7.1, taking $N = 5$ is sufficient). Note that $\mu_N = 1$. Denote the roots of Equation (12) at $\mu = \mu_n$ by $s^{(n)}_{\pm k}$. The solutions $s^{(n)}_{\pm k}$ at all the steps make the trajectories or loci of the eigenvalues.

Based on the above root locus concept, an iterative solution process is devised as follows.

Step 1. For $\mu = \mu_1$ and the initial values $s^{\circ}_{\pm k}$, solve the characteristic Equation (12) by a nonlinear solver (say, the MATLAB function fsolve). This yields the solutions $s^{(1)}_{\pm k}$.

Step 2. For $n = 2, 3, ..., N$, solve Equation (12) with $\mu = \mu_n$ and the initial values $s_{\pm k}^{(n-1)}$. This yields the solutions $s_{\pm k}^{(n)}$. The results obtained in the last step, $s_{\pm k}^{(N)}$, are the eigenvalues of the original lossy transmission line, as shown in Table 1.

The above-described root locus method can be extended to general multiconductor transmission lines.

References

[1] R. E. Collin, *Field Theory of Guided Waves*, 2nd ed. Hoboken, NJ, USA: Wiley-IEEE Press, 1990.

[2] K. D. Granzow, *Digital Transmission Lines: Computer Modelling and Analysis*. Oxford, UK: Oxford University Press, 1998.

[3] C. R. Paul, *Analysis of Multiconductor Transmission Lines*, 2nd ed. Hoboken, NJ, USA: John Wiley & Sons, 2007.

[4] W. Wolf, *Modern VLSI Design: System-on-Chip Design*. Hoboken, NJ, USA: Pearson Education, 2002.

[5] A. Orlandi and C. R. Paul, "FDTD analysis of lossy, multiconductor transmission lines terminated in arbitrary loads," *IEEE Trans. Electromagn. Compat.*, vol. 38, pp. 388–399, 1996. https://doi.org/10.1109/15.536069.

[6] B. Kordi, J. LoVetri, and G. E. Bridges, "Finite-difference analysis of dispersive transmission lines within a circuit simulator," *IEEE Trans. Power Deliv.*, vol. 21, no. 1, pp. 234–242, 2006. https://doi.org/10.1109/TPWRD.2005.855431.

[7] C. Jiao, Z. Xia, and W. N. Fu, "A generalized multiconductor transmission line model and optimized method for the solution of the MTL equations," *Int. J. Antennas Propag.*, vol. 2012, p. 827240, 2012. https://doi.org/10.1155/2012/827240.

[8] E. L. Tan and D. Y. Heh, "Multiple 1-D fundamental ADI-FDTD method for coupled transmission lines on mobile devices," *IEEE J. Multiscale Multiphys. Comput. Techn.*, vol. 4, pp. 198–206, 2019. https://doi.org/10.1109/JMMCT.2019.2945187.

[9] Z. Pantic and R. Mittra, "Quasi-TEM analysis of microwave transmission lines by the finite-element method," *IEEE Trans. Microwave Theory Tech.*, vol. 34, no. 11, pp. 1096–1103, 1986. https://doi.org/10.1109/TMTT.1986.1133505.

[10] R. Lucic, I. Juric-Grgi, and M. Kurtovic, "Time domain finite element method analysis of multi-conductor transmission lines," *Eur. Trans. Electr. Power*, vol. 19, no. 4, pp. 366–377, 2009. https://doi.org/10.1002/etep.366.

[11] J. R. Griffith and M. S. Nakhla, "Time-domain analysis of lossy coupled transmission lines," *IEEE Trans. Microwave Theory Tech.*, vol. 38, no. 10, pp. 1480–1487, 1990. https://doi.org/10.1109/22.58689.

[12] S. L. Manney, M. S. Nakhla, and Q. J. Zhang, "Analysis of nonuniform, frequency-dependent high-speed interconnects using numerical inversion of Laplace transform," *IEEE Trans. Comput.-Aided Design Integr. Circ. Syst.*, vol. 13, no. 12, pp. 1513–1525, 1994. https://doi.org/10.1109/43.331408.

[13] A. Rajhi, S. Ghnimi, and A. Gharssallah, "Transient analysis of the EM field coupling to multi-conductor transmission lines using the NILT method," *Int. J. Microw. Wireless Technol.*, vol. 4, no. 4, pp. 463–472, 2012.

[14] A. K. Agrawal, H. M. Fowles, L. D. Scott, and S. H. Gurbaxani, "Application of modal analysis to the transient response of multiconductor transmission lines with branches," *IEEE Trans. Electromagn. Compat.*, vol. EMC-21, no. 3, pp. 256–262, 1979.

[15] S. Barmada, A. Musolino, and M. Raugi, "Hybrid F.E.-wavelet method for nonlinear analysis of nonuniform MTL transients," *IEEE Trans. Magn.*, vol. 36, no. 4, pp. 977–981, 2002. https://doi.org/10.1109/20.877605.

[16] S. Barmada, "Algebraic solution of time-domain nonuniform transmission-line equations by 2-D wavelet transform," *IEEE Trans. Circ. Syst. I: Fundam. Theory Appl.*, vol. 49, no. 4, pp. 504–508, 2002. https://doi.org/10.1109/81.995666.

[17] J. Chen and L. He, "Modeling and synthesis of multiport transmission line for multichannel communication," *IEEE Trans. Comput.-Aided Design Integr. Circ. Syst.*, vol. 25, no. 9, pp. 1664–1676, 2006.

[18] M. Chilan, A. Pirhadi, and S. Asadi, "Analysis of multiconductor transmission lines using the time domain method of lines," *AEU Int. J. Electron. Commun.*, vol. 138, p. 153863, 2021. https://doi.org/10.1016/j.aeue.2021.153863.

[19] F. Zahedi, E. Mehrshahi, and A. Jahanian, "A closed-form transient response of coupled transmission lines," *IEEE Syst. J.*, vol. 16, no. 1, pp. 801–809, 2021.

[20] S. Soltani, J. Dusenbury, and K. C. Kerby-Patel, "Multiconductor transmission line model for an antenna with high-impedance ground plane," *IEEE Antennas Wireless Propag. Lett.*, vol. 19, no. 12, pp. 2097–2101, 2020. https://doi.org/10.1109/LAWP.2020.3023378.

[21] M. Wulff, T. Hillebrecht, L. Wang, C. Yang, and C. Schuster, "Multiconductor transmission lines for orbital angular momentum (OAM) communication links," *IEEE Trans. Components, Packaging Manuf. Technol.*, vol. 12, no. 2, pp. 329–340, 2022. https://doi.org/10.1109/TCPMT.2022.3140920.

[22] J. L. Rotgerink, R. Serra, and F. Leferink, "Multiconductor transmission line modeling of crosstalk between cables in the presence of composite ground planes," *IEEE Trans. Electromagn. Compat.*, vol. 63, no. 4, pp. 1231–1239, 2021. https://doi.org/10.1109/TEMC.2020.3040689.

[23] M. Chilan, A. Pirhadi, S. Asadi, and S. Helfert, "Analysis of multiconductor transmission lines using the time domain method of lines," *AEU Int. J. Electron. Commun.*, vol. 138, p. 153863, 2021. https://doi.org/10.1016/j.aeue.2021.153863.

[24] M. A. Sobouti, D. Azizian, M. Bigdeli, and G. B. Gharehpetian, "Multi-conductor transmission line model of split-winding transformer for frequency response and disk-to-disk fault analysis," *Int. J. Eng.*, vol. 35, no. 6, pp. 1486–1494, 2021. https://doi.org/10.5829/ije.2021.34.06c.12.

[25] B. Zhao, J. Ou, D. Wang, and Z. Jia, "Analysis of transient response of jointless track circuit based on multiconductor transmission lines theory," *IEEJ Trans. Electr. Electron. Eng.*, vol. 11, pp. 1570–1579, 2022. https://doi.org/10.1002/tee.2366.

[26] H. Wang, B. Gu, G. Zhu, T. Lin, X. Zhao, and W. Duan, "Fast computation method of energization overvoltage in cable lines based on numerical inverse Laplace transform," *J. Phys.: Conf. Ser.*, vol. 2418, no. 1, p. 012056, 2023. https://doi.org/10.1088/1742-6596/2418/1/012056.

[27] N. Duarte, A. De Conti, R. Alipio, and F. Rachidi, "Assessment of the transmission line theory in the modeling of multiconductor underground cable systems for transient analysis using a full-wave FDTD method," *Electric Power Syst. Res.*, vol. 223, p. 109570, 2023. https://doi.org/10.1016/j.epsr.2023.109570.

[28] O. Living, S. N. Nnamchi, M. M. Mundu, K. J. Ukagwu, and A. Abdulkarim, "Coupled modelling and simulation of power transmission lines: a systematic analysis of line losses," *Electric Power Syst. Res.*, vol. 226, p. 109954, 2024. https://doi.org/10.1016/j.epsr.2023.109954.

[29] B. Yang and C. A. Tan, "Transfer functions of one-dimensional distributed parameter systems," *ASME J. Appl. Mech.*, vol. 59, no. 4, pp. 1009–1014, 1992. https://doi.org/10.1115/1.2894015.

[30] B. Yang, *Stress, Strain, and Structural Dynamics: An Interactive Handbook of Formulas, Solutions, and MATLAB Toolboxes*, 2nd ed. Philadelphia, PA, USA: Elsevier Science, 2022.

[31] B. Yang, "Exact transient vibration of stepped distributed systems with mounted lumped masses," *J. Sound Vibration*, vol. 329, no. 8, pp. 1191–1207, 2010.

[32] K. Noh and B. Yang, "An augmented state formulation for modeling and analysis of multibody distributed dynamic systems," *ASME J. Appl. Mech.*, vol. 81, no. 5, p. 051011, 2014. https://doi.org/10.1115/1.4026124.

[33] C. Moler and C. Van Loan, "Nineteen dubious ways to compute the exponential of a matrix, twenty-five year later," *SIAM Rev.*, vol. 45, no. 1, pp. 3–49, 2003.

[34] C. T. Chen, *Linear System Theory and Design*, 4th ed. Oxford, UK: Oxford University Press, 2013.

[35] P. Dyke, *An Introduction to Laplace Transforms and Fourier Series*, 2nd ed. New York, NY, USA: Springer, 2014.

[36] M. R. Spiegel, *Schaum's Outlines: Laplace Transforms*. New York, NY, USA: McGraw-Hill, 1965.

[37] R. T. Irish, "Solution of the telegraphist's equations for coupled transmission lines," *Int. J. Electr. Eng. Educ.*, vol. 15, no. 4, pp. 345–350, 1978. https://doi.org/10.1177/002072097801500412.

[38] J. R. Magnus and H. Neudecker, *Matrix Differential Calculus with Applications in Statistics and Econometrics*, 3rd ed. Hoboken, NJ, USA: Wiley, 2019.

[39] J. C. Butcher, *Numerical Methods for Ordinary Differential Equations*, 3rd ed. John Hoboken, NJ, USA: Wiley, 2016. ISBN-13: 978-1119121503.